Dynamical diffraction of ultrashort X-ray free-electron laser pulses

S. D. Shastri,* P. Zambianchi and D. M. Mills

Advanced Photon Source, Argonne National Laboratory, Argonne, IL 60439, USA. E-mail: shastri@aps.anl.gov

Calculations are presented for the femtosecond time-evolution of intensities of beams diffracted by perfect Bragg crystals illuminated with radiation expected from X-ray free-electron lasers (XFELs) operating through the self-amplified spontaneous emission (SASE) process. After examining the case of transient diffraction of an electromagnetic delta-function impulse through flat, single- and double-crystal monochromators, the propagation of a 280 fs-duration SASE XFEL pulse of 8 keV photons through the same optics is discussed. The alteration of the sub-femtosecond spiky microbunched temporal structure of the XFEL pulse after it passes through the system is shown for both low-order (broad bandwidth) and high-order (narrow bandwidth) crystal reflections. Finally, the shot-to-shot statistical fluctuations of the integrated diffracted intensity is simulated. Implications of these results for XFEL applications are addressed.

Keywords: X-ray free-electron lasers; X-ray sources; X-ray optics; dynamical diffraction.

1. Introduction

Owing to their unique radiation characteristics, planned fourth-generation light sources, *i.e.* X-ray free-electron lasers (XFELs), are expected to extend the applications of X-rays in pure and applied research. The two proposed efforts eventually aiming to produce $\sim$1 Å-wavelength lasing are the LCLS project at SLAC in the USA and a component of the TESLA project at DESY in Germany (LCLS, 2001; TESLA, 2001). Both are linear-accelerator-based sources, employing the self-amplified spontaneous emission (SASE) process that takes place when a highly relativistic dense low-emittance electron beam passes through a long undulator (Madley, 1971). The monochromatic SASE X-rays, having the properties of intense 10^{33} photon s^{-1} (0.1% bandwidth)$^{-1}$ mrad^{-2} mm^{-2} peak brilliance, 1 µrad divergence, 100–300 fs pulse duration, and full transverse coherence, would likely have the most impact in time-resolved studies, coherence-exploiting imaging techniques, and nonlinear X-ray/matter interactions. These unique radiation properties encourage a fresh attempt to understand the performance of current X-ray optics, if used in conjunction with such new sources. This paper examines the transformation of the temporal structure of the XFEL pulse after it passes through simple crystal optics, namely single- and double-crystal reflections, a situation where pulse lengths are comparable with the extinction length scales. It builds upon a previous work by the current authors (Shastri *et al.*, 2001) that examined perfect crystal diffraction responses to delta-function impulse illumination in both Bragg and Laue geometries, looking at transmitted and reflected beams, which, in turn, through a different approach, had extended treatments by others that discussed impulse excitation for the semi-infinite Bragg reflection geometry only (Wark & He, 1994; Chukovskii & Förster, 1995). In the present work, typical 280 fs XFEL pulses with their characteristic sub-fs statistical fine structure (arising from the particle microbunching during the SASE amplification process in the undulator) are simulated and propagated through Si(111) and Si(444) monochromator configurations, corresponding to the lowest- and highest-order reflections accessible in silicon by 8 keV photons. The extent to which the spikes are preserved or smoothed depends on the reflection order (*i.e.* bandwidth), and so also does the shot-to-shot time-integrated intensity. Low-order reflections preserve the intra-pulse spikes and reduce the inter-pulse (shot-to-shot) fluctuations, whereas high-order reflections smooth out the intra-pulse spikes, but increase the inter-pulse fluctuations.

The incompletely understood issue of damage due to the unprecedented peak intensities is a major concern in the subject of XFEL optics. In this study, however, one makes the simplifying assumptions that the crystals are undistorted and that the conventional Ewald–von Laue dynamical diffraction theory (Batterman & Cole, 1964) for perfect crystals is valid. Discussion of the extent to which high-field-induced transient or permanent damage and nonlinear interaction effects invalidate these assumptions is beyond the scope of this presentation. Although damage is believed to be minimized if one uses materials composed of lighter elements (McPherson, 2001), the illustrative calculations here are performed for silicon rather than diamond crystals, which in reality could be the better choice. The selection of silicon over diamond has been made for consistency with the previous work (Shastri *et al.*, 2001) and, within the assumed model, leaves the essential physical results unaffected.

2. Formalism

A Fourier mathematical approach is used to calculate the transient Bragg diffraction response to an incident plane-wave packet propagating towards a crystal at an angle θ_B with respect to the diffracting planes. Let this incident pulse have a time-dependent amplitude

$$E_{\rm inc}(t) = \int_{-\infty}^{\infty} \tilde{E}_{\rm inc}(\omega) \exp(i\omega t)\, {\rm d}\omega$$

at a given point on the crystal surface. The quasimonochromatic reflected pulse will have a mean frequency ω_B whose Bragg angle matches θ_B. The expression for the reflected wave amplitude, at that same point, is

$$E_{\rm ref}(t) = \int_{-\infty}^{\infty} \tilde{E}_{\rm in}(\omega)\, R(\omega) \exp(i\omega t)\, {\rm d}\omega.$$

Here, $R(\omega) = E_H/E_0$ is the frequency-dependent complex amplitude ratio, for the point in question, relating the diffracted wave $E_H \exp(i\omega t)$ to an incident wave $E_0 \exp(i\omega t)$ which arrives along angle θ_B. $R(\omega)$, whose absolute square, after converting frequency into angle, is the well known Darwin–Prins reflectivity curve, can be obtained from steady-state plane-wave dynamical diffraction theory. The time-dependent intensity in the diffracted beam is

$$I(t) \equiv 2\left\langle \left|E_{\rm ref}(t)\right|^2 \right\rangle_{\rm cycle} = \left| 2 \int_0^{\infty} \tilde{E}_{\rm in}(\omega) R(\omega) \exp(i\omega t)\, {\rm d}\omega \right|^2.$$

For a double-reflection geometry composed of two identical crystals, the expressions here are valid provided one replaces $R(\omega)$ with $R(\omega)^2$.

An important special case is the crystal response $E_{\rm ref}(t)$ when the incident pulse is a delta-function $E_{\rm inc}(t) = \delta(t)$. Then, $\tilde{E}_{\rm inc}(\omega) = 1/2\pi$ and the resulting impulse-response amplitude is given by the Green's function

$$G_{\rm ref}(t) = \frac{1}{2\pi} \int_{-\infty}^{\infty} R(\omega) \exp(i\omega t)\, {\rm d}\omega.$$

The expression given earlier for the response $E_{\rm ref}(t)$ to an arbitrary incident pulse $E_{\rm inc}(t)$ can be rewritten alternatively as a continuous superposition of Green's functions at all times in the form of a convolution integral,

$$E_{\rm ref}(t) = \int_{-\infty}^{\infty} E_{\rm inc}(\tau)\, G_{\rm ref}(t-\tau)\, {\rm d}\tau,$$

which represents a temporal smearing of the incident pulse's amplitude by the Green's function.

3. Impulse responses

The $G_{\rm ref}(t)$ responses to incident delta-function inputs are very instructive in formulating an understanding of ultrashort pulse diffraction by crystals, particularly when the duration of, or temporal structure within, the pulse is comparable with the extinction length scale (femtoseconds) of the reflection. Shastri *et al.* (2001) presents impulse responses for single crystals in various Bragg and Laue geometries. Here, the results for the symmetric Bragg case will be reproduced for the two single-crystal reflections Si(111) and Si(444), oriented to select 8 keV radiation from a σ-polarized incident impulse. Responses will also be shown here for double-reflection geometries, as typically used for monochromatization of synchrotron radiation.

Fig. 1 shows the reflected responses (in arbitrary units) of 10 μm-thick Si(111) crystals, in single- and double-reflection configurations, to a delta-function impinging at time $t = 0$ along $\theta_{\rm B} = 14.3^\circ$, which is the Bragg angle for 8 keV X-rays. For the single-reflection case, the transient intensity begins with a discontinuous jump at $t = 0$, reaches its maximum after a few attoseconds, and then decays away in 5 fs. Also noticeable is the presence of a less intense delayed flash at around 16.5 fs, which is an X-ray echo from the back surface of the crystal. This echo becomes stronger and occurs earlier as the crystal thickness is reduced. Interesting in itself, however, the presence of this echo would become relevant in reality only if the incident X-ray pulses are compressed or sliced (Tatchyn & Bionta, 2001; Bionta, 2000; Bucksbaum & Merlin, 1999) to durations less than 10 fs. Fig. 1 also shows the time evolution of diffraction after a Si(111) double-crystal set-up excited by the same incident impulse. The presence of the second crystal has the effect of delaying the transient response further by a few femtoseconds. Although this two-crystal calculation was intellectually motivated by the parallel (nondispersive) geometry conventionally used for synchrotron X-ray monochromators, the response result is valid, in this case, for the dispersive arrangement as well, owing to the assumption of a zero-angular-divergence incident pulse combined with the collimation-preserving property of symmetric Bragg reflections (unlike asymmetric Bragg or Laue reflections) when subjected to polychromatic radiation.

Results of similar impulse response calculations are presented in Fig. 2 for Si(444) single- and double-reflections, for which $\theta_{\rm B} = 81.3^\circ$, assuming semi-infinitely thick crystals. The time dependences have the same profiles as those for Si(111), except that the durations of the 'ringing' excited by delta-function electromagnetic pulses are much longer for the Si(444) case. For 8 keV X-rays, Si(444) has an energy acceptance $\Delta E = 41.4$ meV, significantly smaller than the value $\Delta E = 1.1$ eV for Si(111). Based on these values and the uncertainty relation $\Delta E \Delta t/(2.35)^2 > \hbar/2$, one estimates a response time Δt of a few tens of femtoseconds for Si(444), but just a few femtoseconds for Si(111), consistent with the exact calculations. Finally, note that owing to the treatment of semi-infinite Si(444) crystals, the effect of the back face echo is nonexistent.

4. Response to a SASE XFEL pulse

XFEL physics computer simulations pertaining to planned ∼1 Å-wavelength sources show that, starting from electron density fluctuation noise, the SASE process can generate, after saturation has been achieved, an X-ray pulse length of about 300 fs containing many hundreds of intensity spikes (micropulses) randomly distributed over the full pulse (Fig. 3*a*). The pulse repetition rate is expected to be around 120 Hz and 55 kHz for the LCLS and TESLA machines, respectively (LCLS, 2001; TESLA, 2001). Although the output X-ray beam is fully transversely coherent, the longitudinal coherence is limited only to within the duration of a typical individual spike, which lasts a fraction of a femtosecond. In order to simulate the crystal reflection of an incident 8 keV XFEL pulse, the latter has been approximated here as consisting of $N = 500$ spikes randomly positioned within a 280 fs time window. Each spike is identical and is represented as a Gaussian intensity envelope (with $\sigma = 0.1$ fs) that

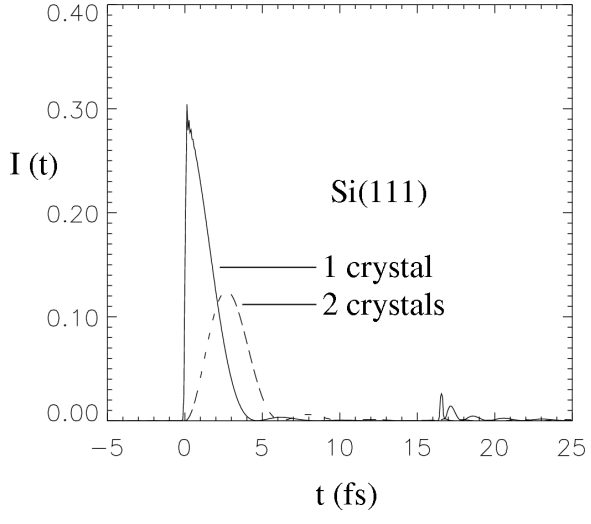

Figure 1
Delta-function-induced transient reflected intensity at 8 keV from one and two Si(111) Bragg crystals of thickness 10 μm.

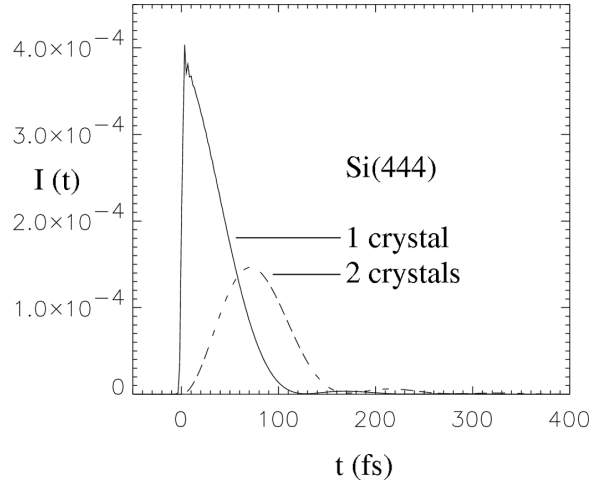

Figure 2
Delta-function-induced transient reflected intensity at 8 keV from one and two Si(444) Bragg crystals of semi-infinite thickness.

modulates a rapidly oscillating electromagnetic field having the 8 keV X-ray frequency ω_r. So, mathematically one has

$$E_{\rm inc}(t) = {\rm Re}\sum_{i=1}^{N} A_i \exp\left[-(t-t_i)^2/4\sigma^2\right]\exp\left[i\omega_r(t-t_i)\right]$$

for a SASE radiation pulse, where the spike amplitudes A_i and occurrences t_i are generated randomly. A single simulated XFEL pulse's structure in the time and frequency domain are shown in Fig. 3 for a particular random set of A_i, t_i. The single-shot spectrum is also characterized by many spikes, all under a 7.8 eV-wide Gaussian envelope corresponding to the Fourier transform spectrum of the wave train within a single coherent micropulse. After many shots the average spectrum smooths out to become the envelope itself.

Passing such a wave train of spikes through a system of crystal optics results in the temporal stretching of each spike by the delta-function response time of the optics. Furthermore, the stretching forces the interference of spikes that were previously adjacent, but not necessarily overlapping. So the resultant outgoing wave train is a smoothed version of the incident one, further modified by accidental degrees of constructive/destructive interference among stretched neighboring spikes.

Fig. 4 shows the time response of single- and double-Si(111) reflection optics (again symmetric Bragg, 10 µm-thick crystals) to the incident pulse in Fig. 3. The diffracted radiation still has strong intensity fluctuations, but slightly less so than the incident pulse, owing to the smoothing influence of the reflections. The smoothing effect is slightly greater in the case of the double-reflection geometry, as expected from the more delayed Green's function response for the two-crystal system (Fig. 1). Note that, owing to the considerable duration of the XFEL pulse relative to the impulse response, the single-crystal's back face echo is washed out and hence not discerned.

Similarly, the transient diffraction from single- and double-Si(444) reflections (symmetric Bragg, semi-infinitely thick crystals) is shown

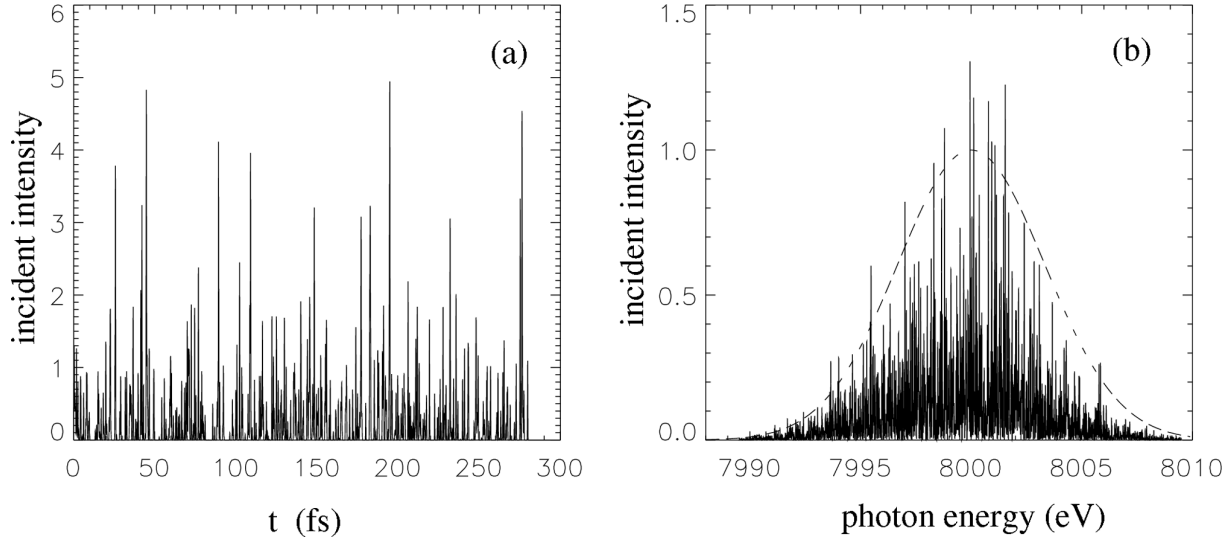

Figure 3
Simulation of a single incident 8 keV XFEL SASE pulse with 500 micropulses in time (*a*) and its Fourier transform spectrum (*b*).

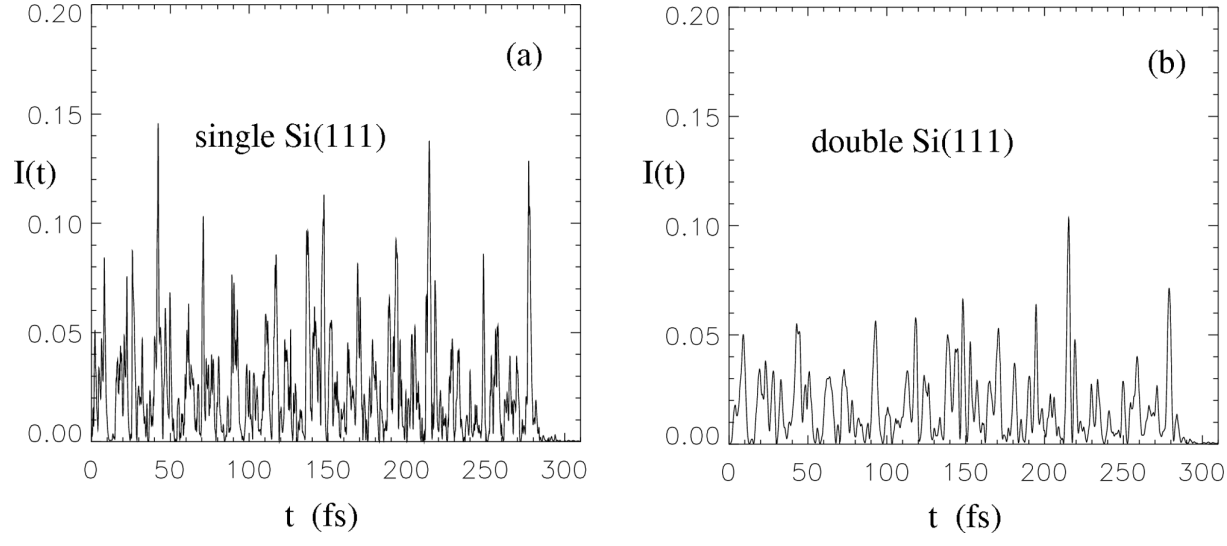

Figure 4
Time-dependent diffraction of the simulated 8 keV XFEL pulse by one (*a*) and two (*b*) Si(111) reflections.

in Fig. 5, again for the same incident XFEL pulse in Fig. 3. The smoothing of the incoming intensity fluctuations is much more dramatic here than for the Si(111) optics, as expected from the considerably longer impulse response durations for the Si(444) case (Fig. 2). Nonzero diffracted intensity persists long after the instant $t = 280$ fs at which the incident pulse ends, up to 350 fs and 400 fs for the single- and double-Si(444) reflections, respectively.

5. Shot-to-shot integrated intensity fluctuations

The statistical aspects of the shot-to-shot fluctuations in the time-integrated intensity,

$$F = \int I(t)\,\mathrm{d}t,$$

are an important consideration for combined XFEL source/monochromator systems. Integrated intensities were simulated for 400 pulses, and the results are displayed in Fig. 6 for Si(111) and Si(444) double-reflection configurations. The relative root-mean-square fluctuations are clearly greater after the high-order Si(444) optics. Quantitatively, for the current 400-shot sampling, one obtains $\Delta F_{\rm rms}/\langle F\rangle = 12\%$ for Si(111) and $\Delta F_{\rm rms}/\langle F\rangle = 56\%$ for Si(444). These results are easily understood by frequency domain considerations. The double-crystal energy-integrated bandwidth $\hbar \int |R(\omega)|^4\,\mathrm{d}\omega$ for Si(111) is 32 times that of Si(444), *i.e.* 0.95 eV as opposed to 30 meV. So the narrow bandwidth energy acceptance window of the higher-order Si(444) reflection intercepts only three to four spikes in a single incident pulse's spectrum (*e.g.* Fig. 3*b*), making its throughput very susceptible to variations. On the other hand, the Si(111) window filters through a much wider band of the incident spectrum and has a

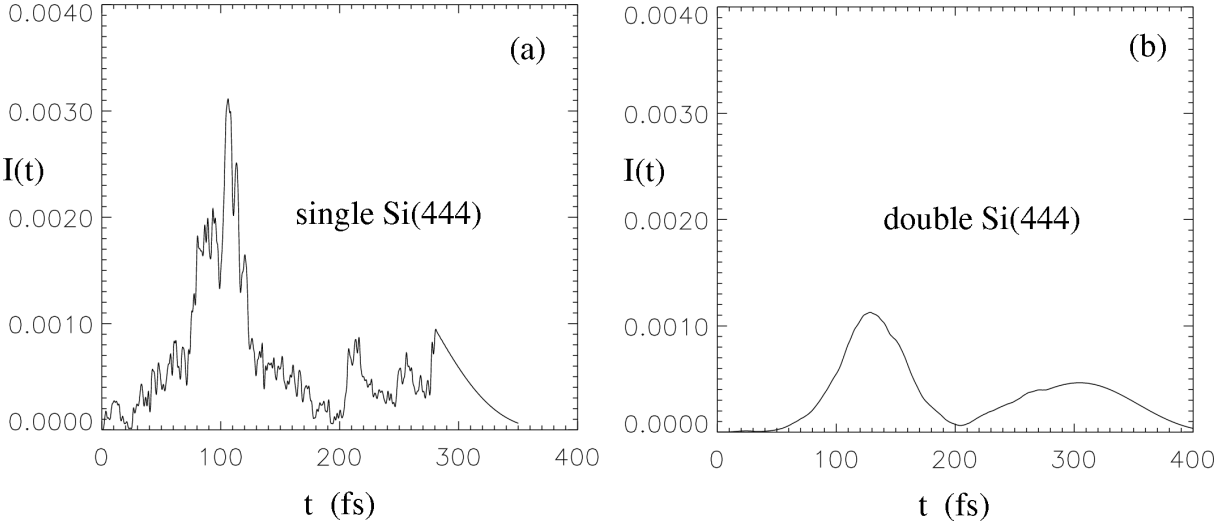

Figure 5
Time-dependent diffraction of the simulated 8 keV XFEL pulse by one (*a*) and two (*b*) Si(444) reflections.

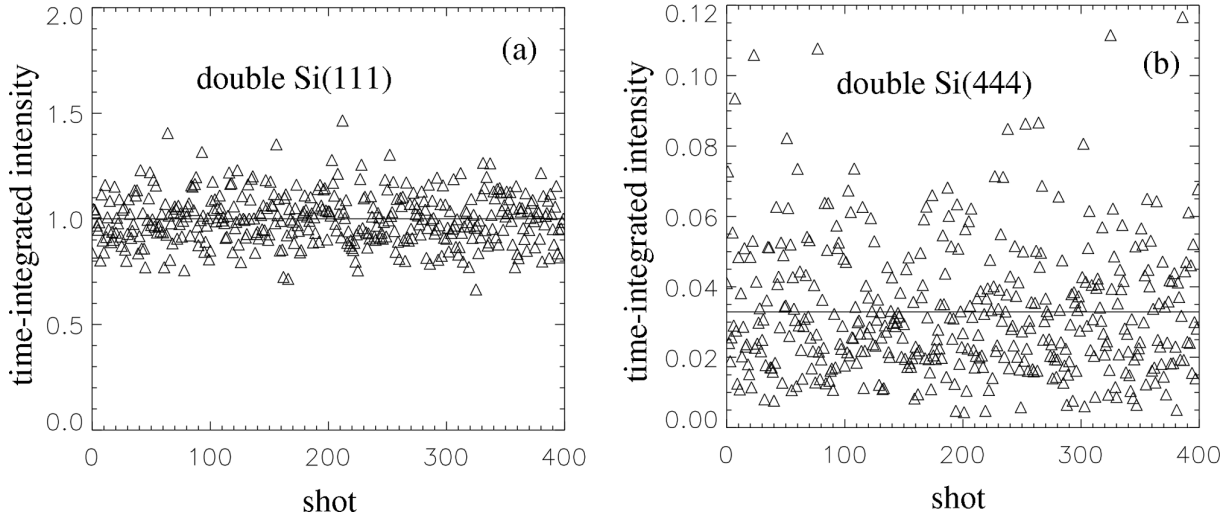

Figure 6
Time-integrated diffraction intensities simulated for 400 XFEL shots after Si(111) (*a*) and Si(444) (*b*) double-crystal monochromators. Horizontal lines show the average values.

throughput that is relatively insensitive to the pulse-to-pulse differences in spectral fine structure. This also explains the average 30-fold weakness of integrated intensity for the Si(444) shots relative to the Si(111) shots.

6. Concluding remarks

A necessary, but nontrivial, refinement of the present work is to incorporate into the treatment a proper description of how the extremely high peak X-ray fields from an XFEL distort the perfect crystal optics and alter their diffraction properties. Under the simple assumptions of undistorted crystals and standard dynamical diffraction theory, this article has addressed three issues pertaining to perfect crystal diffraction of ultrashort XFEL pulses. These are the Green's function responses, the modification of the SASE pulses by the optics, and the shot-to-shot diffracted flux variances. The Green's functions (responses to incident delta-functions), which offer important insights into the regime where pulse durations are comparable with extinction lengths, have properties [*e.g.* echos in thin Bragg and Laue crystals (Shastri *et al.*, 2001)] that would be of experimental relevance if XFEL pulses become compressed or sliced (Tatchyn & Bionta, 2001; Bionta, 2000; Bucksbaum & Merlin, 1999) to $\sim$ 10 fs levels for time-resolved studies.

The extent to which the fluctuations within a single SASE pulse are smoothed by various crystal reflection orders is important if XFEL diagnostics are performed after such optics. These considerations also enter if one conducts experiments where the proper normalization for the measured signal or event rate of interest is not the time-averaged intensity but the instantaneous intensity raised to a higher power, and then averaged. For a nonlinear multiphoton process involving n-photon annihilation, the event rate is proportional to the time-average $\langle I(t)^n \rangle$. For example, two-photon absorption and second harmonic scattering correspond to $n = 2$.

Finally, the shot-to-shot integrated intensity fluctuations after a monochromator can play a role in XFEL applications where sample damage or other constraints motivate techniques that extract the desired information in very few (or even single) shots (Neutze *et al.*, 2000). The severe increase in shot-to-shot variances due to high-order reflection monochromators will also be an issue in so-called seeded-XFEL schemes where the output radiation from a first SASE undulator is highly monochromated using narrow bandwidth crystal optics and then delivered to electrons in a second undulator, where it seeds the microbunching process without it having to evolve from self-amplified electron density noise.

This work was supported by the US Department of Energy, Basic Energy Sciences, Office of Science, under Contract No. W-31-109-Eng-38.

References

Batterman, B. W. & Cole, H. (1964). *Rev. Mod. Phys.* **36**, 681–717.
Bionta, R. (2000). Technical Note LCLS-TN-00-7. Stanford Linear Accelerator Center, CA 94025, USA.
Bucksbaum, P. H. & Merlin, R. D. (1999). *Solid State Commun.* **111**, 535–539.
Chukovskii, F. N. & Förster, E. (1995). *Acta Cryst.* A**51**, 668–672.
LCLS (2001). LCLS project information and publications are available at the internet website http://www-ssrl.slac.stanford.edu/lcls
McPherson, A. (2001). *Proc. SPIE*, **4143**, 20–25.
Madley, J. (1971). *J. Appl. Phys.* **42**, 1906–1913.
Neutze, R., Wouts, R., van der Spoel, D., Weckert, E. & Hajdu, J. (2000). *Nature (London)*, **406**, 752–757.
Shastri, S. D., Zambianchi, P. & Mills, D. M. (2001). *Proc. SPIE*, **4143**, 69–77.
Tatchyn, R. O. & Bionta, R. (2001). *Proc. SPIE*, **4143**, 89–97.
TESLA (2001). TESLA project information and publications are available *via* the DESY internet website http://www-hasylab.desy.de
Wark, J. S. & He, H. (1994). *Laser Part. Beams*, **12**, 507–513.

 Received 23 April 2001 • Accepted 18 July 2001